Introduction to Ultra Wideband Impulse Radio

Dayan Adionel Guimarães & Geraldo Gil Ramundo Gomes

***Abstract*—In this tutorial paper, the basic principles of the ultra wideband impulse radio (IR-UWB) technology are covered. Pulse construction and signaling formats are discussed, along with channel models suited to the IR-UWB system design and assessment. Some reception techniques are also presented, with emphasis on the time reversal. The paper also highlights some applications of the IR-UWB technology.**

***Index Terms*—**Impulse radio, ultra wideband, IR-UWB**.**

***Resumo*—Neste artigo tutorial são apresentados os princípios básicos sobre a tecnologia de radio de banda ultra larga por pulsos, conhecida como IR-UWB. Discute-se sobre a construção dos pulsos de transmissão, bem como sobre algumas das formas de sinalização mais comuns e modelos de canal adequados ao projeto e à avaliação de desempenho de sistemas IR-UWB. São também apresentadas algumas técnicas de recepção de sinais UWB, com ênfase na técnica de reversão temporal. O artigo também aborda algumas aplicações da tecnologia IR-UWB.**

***Palavras chave*—**Banda ultra larga, rádio por pulsos, IR-UWB.

I. INTRODUCTION

In ultra wideband impulse radio (IR-UWB) technology [1], very short energy pulses, typically on the order of hundreds of picoseconds, are transmitted with the use of a specially designed wideband antenna [2]. In addition to the low power spectral density, commercially available IR-UWB systems must have very low effective radiated power (ERP), typically in the sub-milliwatt range [3]. The USA Federal Communications Commission (FCC) defines a UWB device "as any device where the *fractional bandwidth* is greater than 0.25 or occupies 1.5 GHz or more of spectrum". The formula proposed by the Commission for computing the fractional bandwidth is $2(f_H - f_L)/(f_H + f_L)$ where f_H is the upper frequency of the –10 dB emission point and f_L is the lower frequency of the –10 dB emission point. The center frequency of the transmission was defined as the average of the upper and lower –10 dB points, i.e., $(f_H + f_L)/2$ [4]. Clearly, the above definition does not restrict UWB to impulse radio transmissions and, as a consequence, other techniques that do not use baseband pulses are currently being considered as candidates for using the UWB spectrum [4][5].

Impulse radio principles date back to the early days of wireless technology, with experiments of the German physicist Heinrich Rudolf Hertz in the 1880's, and with impulse transmissions made by the Italian-born radio pioneer Guglielmo Marconi in 1901 [3]. Nevertheless, impulse radio is being considered as a potential technology for some next generation wireless networks [6]. As a matter of fact, IR-UWB is currently the basis of one of the physical layers specified by the IEEE 802.15.4a standard [7] and encounters applications in cognitive radio (CR) systems [9][10][11]. Besides communications applications, other envisaged uses of IR-UWB are imaging systems, including ground penetrating radar (GPR), wall and through-wall imaging, surveillance and medical imaging devices, measurement systems and vehicular radar [3][4]. Other applications of IR-UWB technology are discussed in [12, Chap. 9].

In this paper, which is pretty much grounded on [13][1] and references therein, the basic principles of the ultra wideband impulse radio technology are covered. Special focus is put on IR-UWB signaling formats, on channel models suitable for IR-UWB system design and simulation, and on detection techniques adopted as a function of the modulation and the channel characteristics. Additional material can be found in the papers [1], [3], [14] and [15] and the books [12], [16], [17], [18], [19] and [20]. We give special credit to the tutorial paper [21]. Papers published in a special issue of the IEEE Transactions on Vehicular Technology on UWB are also worth reading [22].

The remaining of the paper is organized as follows: in Section II some IR-UWB transmission techniques are presented. Section III deals with IR-UWB channel models and Section IV is devoted to the reception of IR-UWB signals. In Section V, some applications of the IR-UWB technology are briefly covered. Section VI concludes the paper.

II. IR-UWB SIGNALING TECHNIQUES

There are essentially two UWB signaling families, one based on continuous transmission of multi-carrier signals and the other based on the transmission of short baseband pulses. In this paper we shall concentrate on the last one, which is commonly referred to in the literature as impulse radio UWB. We use the nomenclature UWB (without the IR prefix) to refer to both continuous and pulsed transmissions.

In what concerns the analysis of the error probability of the signaling schemes presented here, we shall briefly discuss the performance of a single-user system over the AWGN channel. The corresponding analysis for a multiuser environment and over AWGN and multipath fading channels is quite involved and is beyond the scope of this paper. The interested reader

Manuscrito recebido em 20 de dezembro de 2011; revisado em 18 de janeiro de 2012.

D.A. Guimarães (dayan@inatel.br) e G.G.R. Gomes (ge@inatel.br) são professores do Instituto Nacional de Telecomunicações - Inatel. Av. João de Camargo, 510 - Santa Rita do Sapucaí - MG - Brasil - 37540-000.

[1] The reproduction of parts of the text and figures of [13] in this paper was made under written permission of Springer Verlag, Inc.

can find related information in, for example, [23], [24], [25], [26], [14] and [15], or can resort to some generic procedures for the derivation of the error probability in these environments. A rich source of such procedures is the book by M. K. Simon and M.-S. Alouini [27].

Before entering into the specifics of each signaling scheme, some details about the IR-UWB pulse shape are presented in the next subsection.

A. IR-UWB Pulse Shape Design

Impulse radio transmissions use short duration pulses whose format must be designed to comply with regulatory spectral emission masks. Due to easy generation, a Gaussian pulse is considered in the majority of the literature. When such pulse is applied to an ideal transmitting antenna, it is converted into a Gaussian *monocycle* by the derivative behavior of the antenna. This monocycle can be written as [3]

$$p(t) = -2\pi f_c t \exp\left\{\tfrac{1}{2}\left[1-\left(2\pi f_c t\right)^2\right]\right\} \qquad (1)$$

where f_c is the approximate center frequency of the spectrum of $p(t)$. An ideal receiving antenna will differentiate the received electric field monocycle, delivering to the load the second derivative of the Gaussian pulse.

Fig. 1 illustrates the shape and the frequency content of the monocycle for some values of f_c. Note that $f_c = 1/\tau$, where τ is the approximate pulse duration. The power spectral densities of the monocycles were computed from

$$P(f) = \left(f/f_c\right)\exp\left\{\tfrac{1}{2}\left[1-\left(f/f_c\right)^2\right]\right\} \qquad (2)$$

As pointed out in [16, p. 104], a monocycle pulse does not fully comply with the FCC spectral masks for UWB. Possible solutions to this problem are to synthesize different pulse shapes or reshape a Gaussian monocycle through filtering. Nevertheless, the actual responses of the transmitting and receiving antennas must also be taken into account, since the transmitted pulse shape contained in the radiated electric field will differ from the Gaussian monocycle. Examples of pulse design for IR-UWB systems can be found in [16, Chap. 4] and [12, Chap. 6]. In spite of the spectral compliance problem mentioned above, without loss of generality we shall consider in this section the Gaussian monocycle as the reference pulse shape from the perspective of the IR-UWB system building blocks.

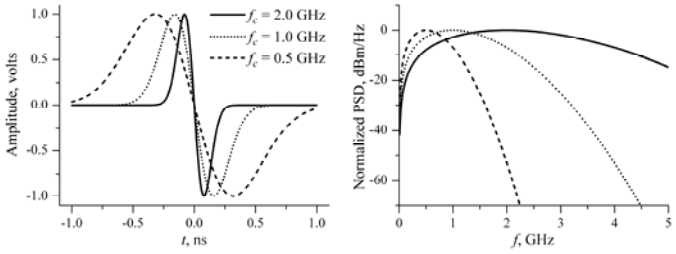

Fig. 1. Gaussian monocycles and their spectral content for different center frequencies.

B. Generic IR-UWB transmitted signal

The IR-UWB signal from the k-th user can be written in the generic form

$$s^{(k)}(t) = \sum_{j=-\infty}^{\infty} \sqrt{\frac{E}{N_s}}\, d_j^{(k)} \beta_{\lfloor j/N_s \rfloor}^{(k)} p\left(t - jT_f - c_j^{(k)} T_c - \delta\alpha_{\lfloor j/N_s \rfloor}^{(k)}\right) \qquad (3)$$

where E is the average energy per symbol, N_s is the number of IR-UWB pulses per symbol and $p(t)$ is the IR-UWB pulse shape [16, p. 79] [14] [15]. A symbol with duration T is divided into frames of duration T_f. The frame duration is typically much larger than the monocycle width, resulting in a signal with a very low duty cycle, which is characteristic of impulse-radio-based UWB systems. The frames of duration T_f are further divided into chips of duration T_c. Inside each frame, the IR-UWB pulse is shifted in a pseudo-random fashion under the control of a user-dependent pseudo-random code $c^{(k)}$ whose elements are positive integers that determines the chip interval in which the IR-UWB pulse will be positioned inside a frame. The time shifts produced by $c^{(k)}$ are called *time hopping* and they are used to avoid *catastrophic collisions*[2] in a multiuser environment [14] [15]. IR-UWB systems that use $c^{(k)}$ implements time-hopping multiple-access and are called time-hopping ultra wideband (TH-UWB) systems.

Continuing the description of the variables in (3), $d^{(k)}$ is a binary bipolar user-specific code used when a *direct-sequence* ultra wideband (DS-UWB) multiple-access scheme is desired. The variable $\beta^{(k)}$ changes the amplitude of the IR-UWB pulses and is associated to *pulse-amplitude modulation* (PAM), *on-off keying* (OOK) and *binary phase-shift keying* (BPSK) IR-UWB systems. The composite variable $\delta\alpha^{(k)}$, where δ is the modulation index and $\alpha^{(k)}$ is the user data symbol number, produces time-shifts that are added to the time-hopping pattern produced by $c^{(k)}$, and is used in the implementation of *pulse-position modulation* (PPM) IR-UWB systems. Note that $\alpha^{(k)}$ and $\beta^{(k)}$ changes every N_s hops, since each symbol carries N_s IR-UWB pulses. Then, the index of the data symbol modulating a IR-UWB pulse j is the integer part of j/N_s, represented in (3) by $\lfloor j/N_s \rfloor$. Finally, the pulse shape $p(t)$ can also be changed according to the symbol to be transmitted to form a *pulse-shaping modulation* (PSM) IR-UWB system.

We are now able to specialize (3) for some signaling techniques and to analyze some specific details about each of them. We shall consider the time-hopping version of the IR-UWB signaling schemes, which means that in what follows we consider $d^{(k)} = 1$ in (3).

C. PPM Signaling

There are two types of PPM signaling for IR-UWB applications: *orthogonal PPM* and *optimum PPM*. In both cases the chip duration is equal to the IR-UWB pulse duration. However, in orthogonal PPM pulse positions do not overlap, meaning that their correlation is zero. In optimum PPM, the IR-UWB pulse positions are spaced δ_{opt} seconds apart, where

[2] In a catastrophic collision, a large number of pulses from two or more signals are received at the same time instants [14].

δ_{opt} is the value of δ that maximizes $R_p(0) - R_p(\delta)$, where $R_p(\delta)$ is the normalized autocorrelation function of the IR-UWB pulse $p(t)$, the normalization being relative to the IR-UWB pulse energy.

The Fig. 2 shows the autocorrelation function of three IR-UWB pulses formed by derivatives of the Gaussian monocycle. In orthogonal PPM we have $\delta = T_c$, guaranteeing a zero correlation. In optimum PPM, δ_{opt} will depend on the pulse shape. Observe in Fig. 2 that, if the conventional monocycle $p(t)$ defined in (1) is used, the optimum value of δ is around $0.4T_c$. Nevertheless, if the third derivative of the Gaussian pulse is used, the optimum separation decreases to around $0.25T_c$, increasing the power efficiency of the system.

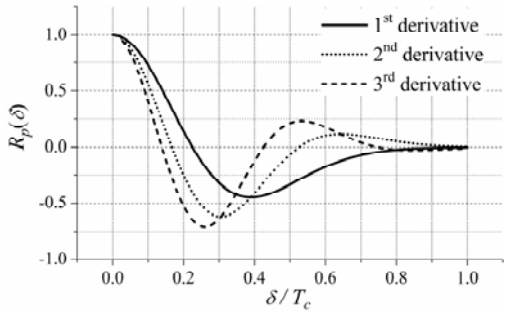

Fig. 2. Autocorrelation function of different IR-UWB pulses derived from a Gaussian monocycle.

A binary time-hopping orthogonal PPM (TH-PPM) signal can be generated from (3) by making $\beta^{(k)} = 1$, $\delta = T_c$ and the binary symbol numbers $\alpha^{(k)} = 0$ or 1, depending on the user data bit. In a optimum PPM, $\beta^{(k)} = 1$, $\delta = \delta_{opt}$ and the binary symbol numbers $\alpha^{(k)} = 0$ or 1, depending on the user data bit.

The average symbol error probability of a single-user binary orthogonal PPM IR-UWB over the AWGN channel is identical to the symbol error probability of the binary orthogonal FSK signaling analyzed in [13, Chap. 6], with E_b, the average energy per bit, equal to N_s times the IR-UWB pulse energy. The average symbol error probability of a single-user optimum binary TH-PPM IR-UWB is obtained similarly, taking into account the pulse correlation, yielding

$$P_e = \frac{1}{2}\operatorname{erfc}\left(\sqrt{\frac{E_b}{2N_0}\left[R_p(0) - R_p(\delta_{opt})\right]}\right) \qquad (4)$$

where E_b is the average energy per bit, equal to N_s times the IR-UWB pulse energy, and N_0 is the noise power spectral density. Observe that $R_p(0) - R_p(\delta) = 1$ for orthogonal PPM and that, in this case, (4) specializes to the expression for the average symbol error probability of the binary orthogonal TH-PPM.

Multilevel TH-PPM signaling techniques can be achieved by allowing $\alpha^{(k)}$ assume values other than 0 and 1. For example, a quaternary TH-PPM signaling can use $\{\alpha^{(k)}\} = 0$, 1, 2 or 3, depending on the symbol to be transmitted. Again, $\delta = \delta_{opt}$ for an optimum multilevel TH-PPM and $\delta = T_c$ for an orthogonal multilevel TH-PPM. The error rate performance of an orthogonal multilevel TH-PPM over the single-user AWGN channel is equal to the performance of any M-ary orthogonal signaling in the same environment [28, p. 436], as derived in [13, Chap. 6] for the M-ary FSK.

D. BPSK Signaling

A time-hopping binary phase-shift keying (TH-BPSK) IR-UWB signal can be generated from (3) by making $\beta^{(k)} = \pm 1$ and $\delta = 0$. This will only invert or not the IR-UWB pulses in a given symbol interval, depending on the user data bit.

The error rate performance of a TH-BPSK signaling over an AWGN channel and in a single-user environment is identical to the performance of an antipodal signaling, as derived in [13, Chap. 6].

E. Bi-Orthogonal Signaling

An M-ary bi-orthogonal signaling is based on the use of $M/2$ orthogonal signals along with their negatives [28, pp. 413-416]. For example, a quaternary bi-orthogonal IR-UWB signaling scheme can be seen as a combination of a binary orthogonal PPM and a binary PSK. The four symbols of a time-hopping quaternary bi-orthogonal signal can be generated from (3) by letting $\delta = T_c$ and by applying the following combinations to $(\beta^{(k)}, \alpha^{(k)})$: (1, 0), (–1, 0), (1, 1) and (–1, 1).

The average symbol error probability of an M-ary bi-orthogonal signaling over the AWGN channel in a single-user environment is given by [28, p. 442]

$$P_e = 1 - \int_{-\sqrt{2E/N_0}}^{\infty}\left[\frac{1}{\sqrt{2\pi}}\int_{-\left(\nu+\sqrt{2E/N_0}\right)}^{\nu+\sqrt{2E/N_0}} e^{-x^2/2}dx\right]^{\frac{M}{2}-1}\frac{1}{\sqrt{2\pi}}e^{-\nu^2/2}d\nu \qquad (5)$$

where $E = E_b \log_2 M$ is the average symbol energy, and where E_b is the average bit energy.

F. PAM Signaling

An M-ary time-hopping pulse amplitude modulation (TH-PAM) signal can be generated from (3) by letting $\delta = 0$ and $\beta^{(k)} = \{a_i\}$, $i = 1, 2, \ldots, M$, where $\{a_i\}$ are the desired IR-UWB relative pulse amplitudes. Note that if $\{a_i\} = \pm 1$, the resultant 2-PAM signaling will be identical to the BPSK signaling previously described.

The average symbol error probability of an M-ary PAM signaling over the AWGN channel in a single-user environment is given by [28, p. 433]

$$P_e = \frac{M-1}{M}\operatorname{erfc}\left(\sqrt{\frac{3E}{\left(M^2-1\right)N_0}}\right) \qquad (6)$$

where $E = E_b \log_2 M$ is the average symbol energy, which is equal to N_s times the IR-UWB pulse energy, and where E_b is the average bit energy.

G. OOK Signaling

The time-hopping on-off keying (TH-OOK) signaling is a special form of TH-PAM in which $\beta^{(k)} = 0$ or a, depending on the user data bit, and $\delta = 0$ in (3). The average symbol error

probability is the same as in the case of a unipolar NRZ signaling [13].

H. PSM Signaling

In pulse-shaping modulation (PSM), different shapes represent the symbols to be transmitted. A time-hopping PSM (TH-PSM) signal can be generated from (3) by letting $\beta^{(k)} = 1$ and $\delta = 0$, changing the pulse shape $p(t)$ according to the user data symbols.

The error rate performance of the TH-PSM signaling is strongly dependent on the choice of the set of waveform shapes $\{p_i(t)\}$, $i = 1, 2, \ldots, M$. Clearly, this fact does not permit us to write a generic expression for the average symbol error probability of a TH-PSM IR-UWB system.

III. IR-UWB Channel Models

In this section a discussion is presented on channel models suited to the design and analysis of IR-UWB systems. The section starts with general aspects of the indoor channel and then moves to specifics of IR-UWB channel models. The section ends with details on a large-scale and a small-scale model that can be adopted for IR-UWB systems.

A. The Mobile Indoor Channel

The study of propagation characteristics inside buildings is not new, but has gained a lot of attention in the past two decades due to the proliferation of indoor wireless communication systems such as wireless local area networks (WLAN) and wireless personal area networks (WPAN).

Both indoor and outdoor channels produce time dispersion due to multipath propagation. As a consequence, they can be described by very similar models. Nevertheless, propagation inside buildings differs from outdoor mainly due to the variety of small-scale obstacles and structures that have *significant* influence on the signal, this influence being increased with an increase in the signal frequency. An outdoor environment seems to be easily handled in this aspect because the effect of small obstacles and structures are averaged-out in a way that they can be taken into account in terms of their average influence on signal propagation. The larger the coverage area and the lower the signal frequency, the more appropriate becomes the assumption of this averaging behavior of the outdoor channel. The indoor channel can be considered a slow time-varying or, in some situations, even time-invariant as compared to the symbol rates of modern communication systems. Time variations occur mainly due to the movement of people nearby the transmitting or receiving antennas, due to the closing or opening of doors and, less frequently, due to the movement of objects during layout modifications. In cases where transceivers are carried by people inside a building, time variations are similar to those produced when these equipments are fixed and people are moving nearby antennas. In these cases very sharp variations in the instantaneous received power (multipath fading) are observed within very small distances. Similarly to the case of the outdoor channel, studies about indoor channels have led to a large amount of models that describe their large-scale and the small-scale propagation mechanisms. See, for example, [29], [30], [31], [32], [33], [34] and [35]. A comprehensive and detailed treatment on the several aspects of the indoor radio propagation is given by H. Hashemi in [36] and by F. Landstorfer, G. Woelfle and R. Hoppe in [37].

B. IR-UWB Channel Models

Much work has been done in the IR-UWB channel modeling arena. Among the uncountable publications we highlight [12, Chap. 4], [18, Chap. 2], [29], [30], [38], [39], [40], [41] and [42], most of them considering indoor propagation.

In terms of large scale propagation, path loss is influenced by effects such as free space loss, refraction, reflection, diffraction and material absorption. In addition to these already know phenomena, IR-UWB propagation also is influenced by *cluttering* and *aperture-medium coupling loss* [12, p. 85]. In a few words, cluttering is the non-organized wave propagation that occurs due to rough surfaces or interfaces. The aperture-medium coupling loss is the difference between the theoretical antenna gain and the gain that is actually realized. It is related to the ratio of scatter angle to antenna beam-width. There is a combination that is worth happening in order to produce a reliable indoor path loss model: an accurate mathematical model, taking into account the electromagnetic propagation fundamentals, and an accurate characterization of the environment in terms of the distribution of the objects between and around a transmitter and a receiver, and in terms of the constituent materials of the several objects. This combination imposes a high involving model, many times intractable in mathematical terms or costly in terms of computational burden for simulation. On the other hand, simple models such as the *log-distance path loss* which is described in this section, seems to produce relatively precise results for the indoor and the outdoor environments. A recent application of the log-distance path loss model in the context of IR-UWB systems is given in [30]. In fact, the overall modeling proposed in [30] was accepted by the IEEE 802.15.4a Task Group as a standard model for evaluating UWB system proposals.

In terms of small scale indoor propagation, the majority of IR-UWB channel models described in the literature use the Saleh-Valenzuela (SV) model [35] or a modified version of it. For this reason, this model is also covered in this section. One of the main modifications in the SV is in terms of the multipath amplitude distribution, which is considered to be log-normal [12] instead of the Rayleigh distribution adopted in [35].

C. The Log-Distance Path Loss Channel Model

Between the transmitter and the receiver terminal, there are a plenty of man-made and natural obstacles that attenuate the electromagnetic signal, causing losses in the average received power. These losses can be divided into distance-dependent and obstacle-dependent terms. The former is an *area-mean* path loss that shows how the distance between the base-station and the mobile terminal affects the area-mean received signal power. The later is a *local-mean* path loss related to the presence of obstacles that impose variations to the local-mean

received signal power about the area-mean received signal power.

The distance-dependent area-mean received power varies normally in a steepest manner than in the free-space scenario, as elaborated in more detail below.

It is known that the *free-space* path loss, in the case where the transmitting and receiving antenna gains are not taken into account, is given by

$$L(d) = 10\log\frac{P_T}{P_R} = -10\log\left[\frac{\lambda^2}{16\pi^2 d^2}\right] \quad \text{dB}, \tag{7}$$

where λ is the wavelength in meters and d is the distance in meters between the transmitter and the receiver. If the transmit and receive antenna gains G_T and G_R, respectively, are included, we have

$$L(d) = -10\log\left[\frac{G_T G_R \lambda^2}{16\pi^2 d^2}\right] \quad \text{dB} \tag{8}$$

In the case of free-space propagation we say that the received power varies inversely proportional to the squared distance. Then we can say that the slope of the free-space attenuation is governed by a *path loss exponent* whose value is $n = 2$. From a real propagation scenario close to the earth surface, it is apparent that the attenuation is not determined by (7) or (8) and that the path loss exponent is greater than 2.

The methods that permit the estimation of the local-mean or area-mean received power at a given distance from the transmitter are generally named *coverage prediction* or *propagation prediction methods*. They vary from the simple log-distance model [43, pp. 138-144] to sophisticated, physics-based 3D ray-tracing and ray-launching methods [44] [45].

There are numerous propagation prediction methods available in the literature, some of which are discussed in survey papers [46] [47] [48] [49]. Most of these methods have been incorporated into software tools that help the process of planning and deployment of wireless communication systems. Several of these tools are briefly discussed in [50]. In spite of the many achievements and publications in the area so far, propagation prediction is still an active research topic, opened for new efforts and contributions. See for example [51], [52] and [53].

We shall study the log-distance propagation prediction method described in [43, pp. 138-144]. The interested reader is invited to consult the references cited above for a discussion on other methods. Before going to the specifics of the log-distance model, a brief discussion about the *two-ray model* might be of great value. This model considers the received signal as composed by a line-of-sight path and a ground-reflected path [43, p. 120] [54, p. 105] [55, p. 64]. Despite of being simple, it is known that this model shows good agreement with empirical data in wireless systems with high towers or predominant line-of-sight. Fig. 3 shows the received power level determined via a two-ray model as a function of the distance between the transmitting tower and the mobile terminal [55, p. 64]. From this figure we can see that two distinct behaviors can be observed in what concerns the slope of the distance-dependent received power. In the left-side of the *critical distance*, the signal strength shows several deep notches as a result of the destructive and constructive interference between the line-of-sight and the ground-reflected paths. On average this signal strength varies following a d^{-2} slope in this region. In the right-side of the critical distance the notches disappear and the signal strength starts to follow a d^{-4} slope. The critical distance, in meters, is approximately determined by

$$d_c = \frac{4h_T h_R}{\lambda}, \tag{9}$$

where h_T and h_R are the transmitting and receiving antenna heights referred to a plane Earth, taking into account the height of the structures or towers where these antennas are installed. The factor λ is the wavelength of the assumed narrowband transmitted signal.

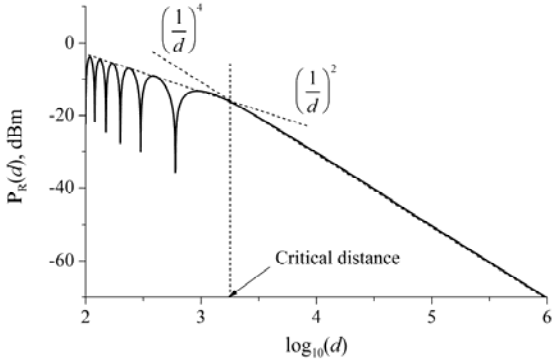

Fig. 3. Received power versus distance calculated from the two-ray model.

Now we are able to construct the log-distance path loss model based on some arguments: in an obstructed area and beyond the critical distance the path loss exponent n will vary, starting from $n = 2$ in the line-of-sight situation with no reflected path. Additionally, if we define a measured area-mean attenuation at a reference distance $d_0 > d_c$, we can write the following area-mean log-distance path loss equation

$$\overline{\overline{L}}(d) = \overline{\overline{L}}(d_0) + 10\log\left(\frac{d}{d_0}\right)^n \quad \text{dB}, \tag{10}$$

where the two bars denote an area-mean, that is, an average taken in such a way that the path loss curve will average-out the influence of the obstacles surrounding the receiver, retaining only the distance-dependent path loss variation.

If we take into account the variations about the area-mean path loss, as caused by the obstacles surrounding the receiver, we can rewrite (10) as

$$\overline{L}(d) = \overline{\overline{L}}(d_0) + 10\log\left(\frac{d}{d_0}\right)^n + X_\sigma \quad \text{dB}, \tag{11}$$

where X_σ is a random variable that corresponds to the fact that at a given distance of the transmitter we may have different *local-mean* attenuations caused by the different configurations

of the surrounding obstacles. Measurements have shown that X_σ is a lognormal random variable with standard deviation σ, in dB. For this reason this variable is usually referred to as a *lognormal shadowing*.

For a better understanding of the lognormal shadowing, consider the following situation: a receiving terminal is moving on a circular path at a constant distance d from the transmitter. From (10), the area-mean received power $\overline{\overline{P}}_R(d)$ will be constant and from (11) the local-mean received power $\overline{P}_R(d)$ will vary about the area-mean following a lognormal distribution. Fig. 4 illustrates a possible behavior of the local-mean received power. On the right-side of the figure a Gaussian probability density function is representing the random variation of $\overline{P}_R(d)$ about its mean $\overline{\overline{P}}_R(d)$. From this density we can notice that, although the log-distance path loss model is not able to predict the values of $\overline{P}_R(d)$, it is able to give statistical information about the lognormal shadowing. For example, it is possible to estimate the probability that the local-mean received power is below or above a given threshold γ, as long as we know the mean $\overline{\overline{P}}_R(d)$ and the standard deviation σ of the lognormal distribution. However, from (10) we notice that the value of the path loss exponent n must also be known.

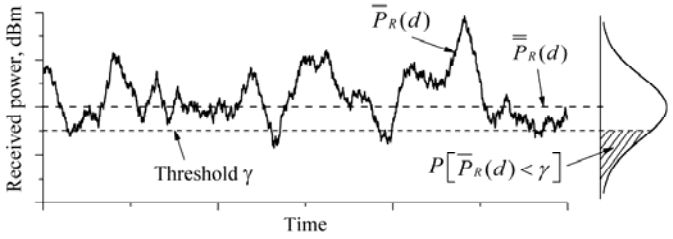

Fig. 4. Illustration of the lognormal shadowing.

Since the standard deviation σ does not depend on the distance, its value and the value of n can be estimated from measurements. The usual method estimates n and σ in such a way that the mean square error (MSE) between the estimated and the measured path losses or received powers is minimized. This MSE is

$$J(n) = \frac{1}{K}\sum_{k=0}^{K-1}\left[P_k - P_k(n)\right]^2 \qquad (12)$$

where K is the number of measurements, P_k is the k-th measured local-mean received power, in dBm, at a given distance d from the transmitter and $P_k(n)$ is the corresponding estimated area-mean received power, also in dBm, whose value will be a function of n and is determined by applying (10). Since $P_k(n)$ is the area-mean estimated received power, then it is the mean of the lognormal distribution of the shadowing. Then, (12) can be seen a (biased) sample variance of the local-mean received power, which allows us to write

$$\sigma = \sqrt{J(n)}\Big|_{n:\,\min \mathrm{MSE}} \quad \mathrm{dB}. \qquad (13)$$

In the notation of (13) we have indicated that the value of n used in $J(n)$ will be the estimated value that minimizes $J(n)$.

Although the knowledge of the above probability is useful, it would be more useful if we were able to know the probability that the local-mean received signal power is above (or below) a certain threshold over the entire circular coverage area of radius d. With this information at hand a service provider can, for example, guarantee that the subscribers will be served within the specified percentage of the coverage area with a received power greater than a threshold (often related to the sensitivity of the receivers). This probability, converted into a fraction of the coverage area, is determined according to [56, p. 127] [43, p. 142]

$$F(\gamma) = \frac{1}{2}\left[\mathrm{erfc}(a) + \exp\left(\frac{1-2ab}{b^2}\right)\mathrm{erfc}\left(\frac{1-ab}{b}\right)\right],$$
$$\text{where} \quad a = \frac{\gamma - \overline{\overline{P}}_R(d)}{\sigma\sqrt{2}} \quad \text{and} \quad b = \frac{10n\log_{10}(e)}{\sigma\sqrt{2}}. \qquad (14)$$

Fig. 5 shows several values of the quotient σ/n and the probability that the received signal power is above the threshold on the circumference (area boundary) of radius d. The percentage of the coverage area with signal strength greater than a given reference threshold can be approximately determined through this figure. First we have to compute σ/n. Starting from this value in the horizontal axis we go up until the curve for the desired $P[\overline{P}_R(d) > \gamma]$ is found. From this point we go to the left and obtain the desired fraction of the coverage area.

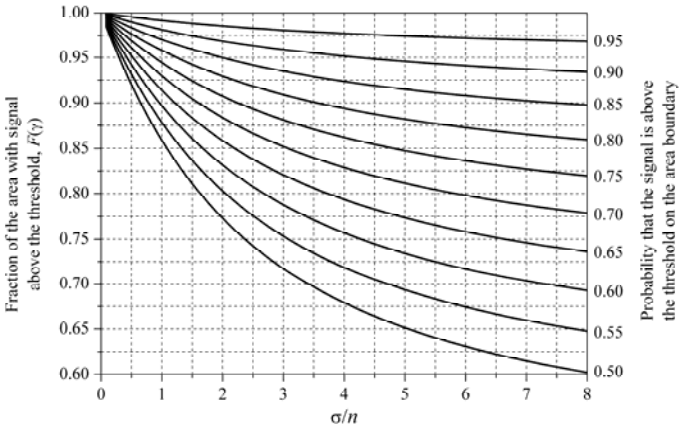

Fig. 5. Fraction of a circular coverage area with signal strength greater than the threshold γ.

D. Further Comments on the Indoor Large-Scale Propagation

Characterizing with precision the large-scale propagation in an indoor environment is a very difficult task, since the number of variables is large and the influence of lots of them can not be precisely quantified in deterministic terms. Just to

mention a few examples, indoor propagation is greatly affected by the physical dimensions of the building and the disposition of its rooms, the material used to construct and cover walls, ceiling and floor, the type, variety, material and layout of the furniture, the position of the transmitter and receiver, the mobility of people nearby and in-between the transmitter and receiver and the frequency of operation.

There are basically five families of models for path loss estimation in indoor channels, as discussed in [36] and [37]. The first four families are narrowband models and the last one is a wideband model:

- In the log-distance path loss model the received power varies inversely proportional to the *n*-th power of the distance between the transmitter and the receiver, *n* being an environment-dependent variable.
- In a variation of the log-distance family of models, the path loss exponent is also distance-dependent.
- Another family of models adopts a log-distance free-space attenuation to which is added the attenuation of various types of structures that can be typically found inside buildings.
- In another family of models the attenuation is given in terms of a unit of distance, for example dB/m or dB/ft. These attenuations are dependent on the characteristics of the building and in some situations they are also described by multiple slopes.
- In the family of models based on wideband pulse transmission, path losses can be estimated from the average power contained in the channel impulse response. Ray-tracing [57] and other modern wideband techniques [37] [44] [45] can be included in this family.

The log-distance path loss model can be used to provide a picture on the problem. Some measurements of the local-mean average received power at several distances from a transmitter are reported in [35]. A linear regression is used to obtain the best fit between the data and the path loss prediction given by the log-distance path loss model. A similar procedure was adopted in [58]. An extensive list of results using the log-distance model has been reported in [36].

Recall from preceding discussions that the log-distance model has two main parameters: the path loss exponent *n* and the standard deviation σ of the local-mean power about the area-mean power. We summarize below some of the results provided in the references cited above in what concerns these parameters and other relevant information on the indoor channel propagation:

- The indoor channel can produce much larger path losses than the outdoor channel.
- Path losses can vary a lot in very short distances from the transmitter. It is possible that most of the accepted attenuation (90 dB or even more) is produced up to 10 meters from the transmitter.
- Indoor channels can not be considered stationary, except in those situations where the movement of people and objects causes variations that can be considered negligible. This situation can occur when people or objects move far away from the transmitting and the receiving antennas.
- Reported values of *n* vary from 1 to 6. Values less than the free space path loss exponent ($n = 2$) correspond to wave-guided signals in hallways and some rooms. These waveguide-like structures are formed in-between the walls and can produce constructive interferences among propagation paths that have small phase differences. Values of *n* on the order of 5 or 6 correspond to situations where the signal has to cross walls with steel beams, ceilings, floors and metalized room partitions.
- The materials used in partitions that have the most influence on the signal attenuation are [37]: metal (26 dB @ 815 MHz), reinforced concrete (10 dB @ 900 MHz and 16 dB @ 1,700 MHz), brick (6 dB @ 900 MHz and 10 dB @ 1,800 MHz) and plywood and glass (less than 3 dB).
- Short coverage distances imply low-power and light transceiver equipments.
- The standard deviation σ of the path loss predicted with the log-distance model was reported to be in the range of 1 dB for predominant line-of-sight propagation to 16.3 dB for all data combined in four buildings, but it is often below 10 dB [36]. This indicates that the log-distance model can be very precise for some buildings (small σ), but can produce very imprecise results in others.

As in the case of the outdoor channel, it seems that there is no coverage prediction model suitable for all types of buildings. Maybe that is the reason for which recent computational planning tools is capable of using several models that can be chosen or combined depending on the analyzed environment.

E. The Saleh-Valenzuela Small Scale Channel Model

Small-scale indoor propagation has a similar definition when compared to the definition adopted for an outdoor channel. It refers to the rapid fluctuations on the instantaneous received power in relatively short distances, typically on the order of less than a wavelength. The main characteristics of the small-scale propagation inside buildings are:

- The channel varies slowly as compared to the outdoor channel, since people inside building move slowly. As a consequence, Doppler shifts are small. However, systems that are using or plan to use frequency bands up to 50 or 100 GHz (millimeter-wave range) can be affected by the Doppler spread even in an indoor environment.
- Typical delay spreads of outdoor channels are on the order of 10 μs up to more than 100 μs in hilly terrains. In contrast, typical maximum absolute delay spreads of indoor environments are below 100 ns, with maximum *rms* delay spreads of about 50 ns [35]. This will lead to high coherence bandwidths and, as a consequence, higher transmission rates can be achieved.
- The number of multipath components in the discrete tapped delay line model is typically a random variable.

- The indoor channel can not be considered stationary in most situations. Then, a wide-sense stationary (WSS) channel model is not always appropriate.
- Adjacent multipath components of the same impulse response can not be considered independent in all instances. Then, an uncorrelated scattering (US) channel model is not appropriate for describing those instances.

A. A. M. Saleh and R. A. Valenzuela proposed a statistical model for indoor multipath propagation based on measurements taken in the first-floor of a medium-size office building [35]. They used radar-like pulses in the 1.5 GHz range to obtain impulse responses within a time resolution of about 5 ns. The work by Saleh and Valenzuela has led to the channel model later named after the authors. It is one of the seminal works about indoor channel characterization, upon which several other important results were built and are used nowadays for designing local area networks and ultra-wideband communication systems.

In the Saleh-Valenzuela model, multipath signals arrive at the receiver in clusters. These clusters are formed due to the building superstructures, like metalized walls and doors. The individual multipath components within a cluster are formed by multiple reflections in objects nearby the transmitter and the receiver, like walls, furniture and people. The amplitudes of the multipath components are Rayleigh-distributed with a variance decaying exponentially with the cluster delay and with the path delay within a cluster. The phase of each multipath component is uniformly-distributed over [0, 2π). The clusters, as well as the multipath components within a cluster form a Poisson arrival process with different and constant arrival rates. As a consequence, the clusters and the individual multipath components have inter-arrival times that are exponentially-distributed [13, Chap. 1].

The impulse response of the channel can be described by a tapped delay line model, resulting in

$$h(t) = \sum_{l=0}^{\infty} \sum_{k=0}^{\infty} \alpha_{kl} \exp(j\theta_{kl}) \delta(t - T_l - \tau_{kl}) \tag{15}$$

where α_{kl} and θ_{kl} are respectively the amplitude gain and the phase rotation for the k-th ray within the l-th cluster, T_l is the arrival time of the l-th cluster and τ_{kl} is the arrival time for the k-th ray within the l-th cluster.

To implement the Saleh-Valenzuela indoor channel model considering a distance d from the transmitter to the receiver, we apply the steps described in what follows. First we need to generate the cluster arrival times according to the conditional exponential distribution

$$p\left(T_l \mid T_{l-1}\right) = \Lambda \exp\left[-\Lambda\left(T_l - T_{l-1}\right)\right], \quad l > 0 \tag{16}$$

where Λ is the *cluster arrival rate* and $T_0 = 0$ is the arrival time for the first cluster. In [35], the mean time between clusters was experimentally found to be $1/\Lambda = 300$ ns.

Let $E[\alpha^2_{kl}]$ denote the average power gain for the k-th ray within the l-th cluster. To proceed we need to estimate the *average first ray power gain* within the first cluster, $E[\alpha^2_{00}]$. This can be achieved by applying a path loss prediction method to obtain the area-mean power loss $\overline{\overline{L}}(d)$. For example, we can use the log-distance method described in Sec. III.A, considering a reference line-of-sight distance d_0 = 1 m [35], and compute in a linear scale:

$$\overline{\overline{L}}(d) = \overline{\overline{L}}(1\text{m}) d^n \tag{17}$$

where $\overline{\overline{L}}(1\text{m})$, instead of measured as in the case of the outdoor propagation, can be estimated with a good precision for an indoor environment by applying the free-space attenuation formula given in (7) or (8). The path loss exponent n can be obtained according to the similarities among the environment under analysis and those for which values of n were reported in [35] or other references. The value of n can also be estimated using the procedure described in Example 3.1 over a set of power measurements inside the building under analysis.

From [35] we can obtain

$$E\left[\alpha_{00}^2\right] = (\gamma\lambda)^{-1} \Big/ \overline{\overline{L}}(1\text{m}) d^n \tag{18}$$

where λ denote the *ray arrival rate* and γ denote the exponential *ray power-decay time constant*. Typical values found for these parameters, as reported in [35], are $1/\lambda$ = 5 ns for the mean time between ray arrivals and γ = 20 ns.

Now we can generate the rays within the clusters with relative arrival times $\{\tau_{kl}\}$ following the conditional exponential distribution

$$p\left(\tau_{kl} \mid \tau_{(k-1)l}\right) = \lambda \exp\left[-\lambda\left(\tau_{kl} - \tau_{(k-1)l}\right)\right], \quad k > 0 \tag{19}$$

The gains $\{\alpha_{kl}\}$ for the k-th ray within the l-th cluster are generated according to a Rayleigh distribution, that is,

$$p\left(\alpha_{kl}\right) = \frac{2\alpha_{kl}}{E[\alpha_{kl}^2]} \exp\left(-\frac{\alpha_{kl}^2}{E[\alpha_{kl}^2]}\right) \tag{20}$$

where $E[\alpha^2_{kl}]$ is computed from the previously estimated value of the average first ray power gain $E[\alpha^2_{00}]$, the ray power-decay time constant γ and the cluster power-decay time constant Γ (adopted equal to 60 ns in [35]) according to

$$E[\alpha_{kl}^2] = E[\alpha_{00}^2] \exp\left(-\frac{T_l}{\Gamma}\right) \exp\left(-\frac{\tau_{kl}}{\gamma}\right) \tag{21}$$

Note that, as established by the model, exponentially decaying paths arrive in clusters that are also exponentially decaying, as illustrated by Fig. 6.

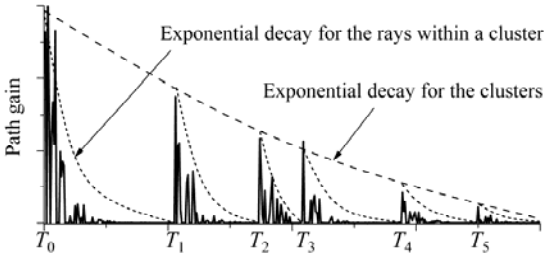

Fig. 6. Illustration of an indoor impulse response generated by the Saleh-Valenzuela model.

The phase for each multipath component is generated according to a uniform distribution over $(0, 2\pi]$:

$$p(\theta_{kl}) = \begin{cases} \dfrac{1}{2\pi}, & 0 < \theta_{kl} \le 2\pi \\ 0, & \text{otherwise.} \end{cases} \tag{22}$$

It is well known that the Rayleigh path amplitudes and uniform phases can be directly generated from two Gaussian random variables X_{kl} and Y_{kl} with zero mean and standard deviation $\sigma = (E[\alpha_{kl}^2]/2)^{1/2}$, according to [13, p. 77]:

$$\begin{aligned} \alpha_{kl} &= \sqrt{X_{kl}^2 + Y_{kl}^2} \quad \text{and} \\ \theta_{kl} &= \arctan\left(Y_{kl} / X_{kl}\right). \end{aligned} \tag{23}$$

The exponential random variables used by the Saleh-Valenzuela model can be easily generated using methods for random number generation like those briefly covered in [13, Chap. 1]. The inverse cumulative distribution method is of particular interest due to its simplicity.

The generation of all random variables described above is necessary but not sufficient to complete the implementation of the Saleh-Valenzuela indoor channel model. Individual creativity must be put into action to make those random variables control the corresponding parameters of the tapped delay line (TDL) model. For example, the exponential random variables described by the probability density functions (16) and (19) must be used to control the time instant that each cluster and each path within a cluster are generated, which corresponds to control the delay blocks in a TDL model. After these instants have been determined, the corresponding Rayleigh path gains and uniform phases are generated to become the multiplicative factors in each TDL arm. These path gains have an exponentially decaying mean square value within a cluster and the cluster has also an exponentially decaying behavior, as determined by (21). Additionally, note from (15) that, in theory, we have an infinite number of clusters and paths. Then, to implement the model we must truncate the TDL to a number of taps enough to represent the lower intensity rays according to what is desired.

IV. Reception of IR-UWB Signals

The energy carried by an IR-UWB pulse is very low, making it difficult to detect a single pulse in a noisy environment. However, the use of several IR-UWB pulses per symbol allows for the detection of the transmitted signals with much higher confidence. This comment allows us to realize that an IR-UWB receiver must be equipped with a number of correlators equal to the number of pulses per symbol. In a multipath fading channel, echoes or replicas of the transmitted pulses are produced, which permits the implementation of a RAKE receiver aiming at collecting most of the energy spread in the time domain. Furthermore, since IR-UWB pulses have very short durations, a fine time resolution can be achieved by the RAKE receiver. Nevertheless, this will happen at a cost of an increased number of taps (and, thus, an increased complexity) to make the overall time span of the RAKE receiver delay line to be comparable to the channel delay spread.

Some of the approaches that can be used to design a IR-UWB receiver are briefly described in the following items. They include optimum and suboptimum solutions. Suboptimum approaches yield a performance penalty, but the receiver can be considerably less complex than the corresponding optimum solution.

- When the system operates over an AWGN channel or over a flat and slow fading channel, no intersymbol interference (ISI) occurs. Additionally, with a time interleaver with sufficient depth[3], the flat fading channel can be considered as memoryless. In this case, the optimum receiver is the *matched filter* or *correlation* receiver, which employs the maximum-likelihood (ML) symbol-by-symbol detection rule [13, Chap. 6].
- When the channel is time-dispersive, as is the case of multipath fading channels, ISI occurs and the optimum receiver uses the *maximum-likelihood sequence estimation* (MLSE) rule [59, p. 584] [19, p. 44]. In this case, the channel output can be represented by a trellis and the MLSE rule estimates the most probable path through the trellis. The Viterbi algorithm is a solution to find this most probable path [59, p. 589].
- Another approach that can be adopted in the multipath fading case is the use of the RAKE receiver employing path diversity with the optimum maximum ratio combining (MRC) rule. In this case, the resolvability of the propagation paths can be viewed as a multichannel system where proper multichannel receiver design rules apply [27, Chap. 9].
- Instead of using a RAKE receiver approach, a suboptimal technique called IR-UWB *transmitted reference* can be applied [60]. This technique is also able to capture the energy available in a IR-UWB multipath channel, but in a simpler way. Basically, a reference IR-UWB pulse is transmitted before each IR-UWB data pulse and, at the receiver side, the received reference portion is correlated with the data portion. For a binary signaling, the polarity of the correlation result is associated to the transmitted data bit and is used for decision. This technique also allows for

[3] The interleaver considered here is responsible for scrambling the transmitted symbols in time so that, after de-interleaving at the receiver side, they appear as having gone through a memoryless channel.

the estimation of the current multipath channel impulse response by the receiver via the probe reference pulses, bringing the possibility of the use of other signal processing techniques for improving system performance.

- In the context of multiuser detection (MUD) in time-hopping (TH) or direct-sequence (DS) IR-UWB systems, the optimum receiver selects the most probable sequence of bits based on the knowledge of all user's codes [59, p. 851] [19, p. 48]. This is equivalent to applying the MLSE rule for all user's signals and form a set of most probable path metrics, then selecting the sequence of bits corresponding to the smallest metric.
- Another approach recently proposed for use in IR-UWB systems is the *time reversal* (or *phase conjugation*) technique [61] [62] [63] [19, p. 47] [64], which was initially considered for applications in underwater acoustic communications [65].

Excepting the time reversal technique, the other ones are typically covered in tutorial material on UWB. For this reason we have decided to bring more details on the time reversal technique in the next subsection. The interested reader can find additional information on the other approaches in the references cited above. In addition to these references, we suggest [16, Chap. 7], [19, pp. 39-51] and [19, Chap. 6].

A. Reception of IR-UWB signals using time reversal

The time reversal technique works by pre-filtering the transmitted signal with a filter whose impulse response is the complex-conjugated and time-reversed version of the channel impulse response (CIR). The composite impulse response, which is formed by the pre-filter in cascade with the channel, can exhibit a concentration of the multipath energy in a smaller (compared to the original CIR) number of *resolvable paths*. This concentration facilitates the subsequent energy capturing process, thus simplifying the receiver at a cost of increasing the complexity of the transmitter. This increased complexity comes from the need of estimating the CIR from a signal transmitted back from the receiver, and from the complexity related to the construction of the pre-filter itself.

Fig. 7 illustrates the idea behind the time reversal technique. User data bits enter the IR-UWB signal generation, which is responsible for generating the sequence of IR-UWB pulses $p(t)$ according to the adopted signaling technique. The IR-UWB signal then goes through a pre-filter whose impulse response $h^*(\mathbf{r},-\tau)$ is the complex-conjugate of the time reversed CIR $h(\mathbf{r},\tau)$. The variable $\mathbf{r}$ is associated to the position of the receiver relative to the transmitter and its presence is included to highlight the strong dependence of the CIR on the receiver position. The received signal enters a matched filter whose impulse response $p(-\tau)*h(\mathbf{r},\tau)$ is matched to the *received* pulse shape. The matched filter output is sampled and the samples are equalized to combat any residual intersymbol interference (ISI). The output of the equalizer is then used in the decision process, which is particular to the signaling technique adopted for the system.

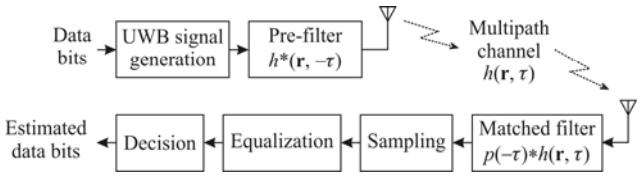

Fig. 7. Conceptual block diagram of an IR-UWB system using the time reversal technique.

Elaborating a little bit more on the concepts behind the time reversal technique, it is known that the convolution of a signal and its complex-conjugate and time-reversed version is equal in shape to the autocorrelation function of this signal. Then, the convolution between $h^*(\mathbf{r},-\tau)$ and $h(\mathbf{r},\tau)$ results in a time-shifted version of the autocorrelation function of the CIR. Fig. 8(*a*) shows the magnitude of a hypothetical indoor channel impulse response and Fig. 8(*b*) shows the convolution $h^*(\mathbf{r},-\tau)*h(\mathbf{r},\tau)$, which is equal to the autocorrelation function of $h(\mathbf{r},\tau)$, except for a time shift. Fig. 8(*b*) illustrates the effect of energy concentration produced by the cascade between the pre-filter and the channel impulse response, which we shall name the *composite channel*. The noticeable peak in the autocorrelation function $h^*(\mathbf{r},-\tau)*h(\mathbf{r},\tau)$ is justified by the highly uncorrelated propagation paths typically encountered in a rich scattering environment. From this function we can see that, although the composite impulse response is longer than the channel response, it has a significant peak capable of concentrating the energy of the received signal scattered in the time domain. The remaining time spread present in the composite channel response must be combated by an equalizer whose complexity, measured in the necessary number of taps, can be reduced compared to an equalizer or a RAKE receiver used in the conventional system. However, there are restrictions imposed to the channel impulse response in a way that the receiver can effectively benefit from the energy concentration capability attributed to the time reversal technique [13]

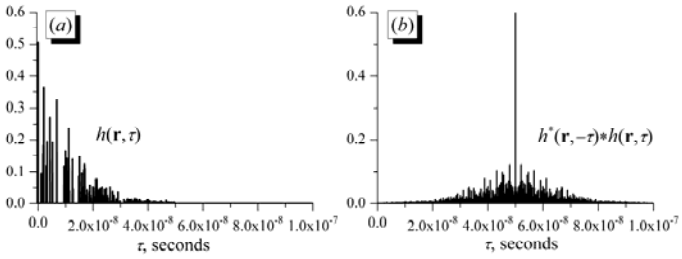

Fig. 8. The effect of energy concentration produced by the time reversal technique: (*a*) A realization of the CIR $h(\mathbf{r},\tau)$, and (*b*) the composite impulse response of pre-filter and CIR.

The possibility of reducing the usable time span of the composite channel impulse response can also allows for an increase in the average pulse repetition rate, which in turn can be translated into an increase in the symbol transmission rate.

It is worth mentioning that the energy concentration not only can manifest in the time-domain. We have already touched this subject when the variable $\mathbf{r}$ in $h(\mathbf{r},\tau)$ was defined. A small change in the relative receiver position can change

significantly the channel impulse response, which means that the correlation $h^*(\mathbf{r}_1,-\tau)*h(\mathbf{r}_2,\tau)$ will be small with high probability. With the help of antenna arrays it is possible to explore this spatial energy concentration to reduce interference from other users in a multiuser IR-UWB system [61][62].

V. Applications of the IR-UWB Technology

As already mentioned, UWB impulse radio is being considered as a potential technology for some next generation wireless networks [6], and is currently the basis of one of the physical layers specified by the IEEE 802.15.4a standard [7]. It also encounters fertile ground in the cognitive radio area [9][10][11]. Other envisaged uses of IR-UWB are imaging systems, including ground penetrating radar, wall and through-wall imaging, surveillance and medical imaging devices, measurement systems and vehicular radar [3][4]. In this section we briefly discuss the above-mentioned applications. Other uses of IR-UWB can be found in [12, Chap. 9], including commercial ones.

A. IR-UWB in the IEEE 802.15.4a Standard

With the main purpose of adding positioning and distancing capabilities to the IEEE 802.15.4 standardization efforts, the UWB impulse radio technology was included in the proposals [7][8]. The IEEE 802.15.4a standard specifies two additional physical layers, one of them using impulse radio time-hoping IR-UWB for frequencies in three ranges: below 1 GHz, between 3 and 5 GHz, and between 6 and 10 GHz. The standard is intended mainly for short-range wireless personal area networks (WPAN).

B. IR-UWB in Cognitive Radio Systems

In [9] it is introduced the concept of cognitive UWB radio, a wireless system based on UWB impulse radio technology and capable of adapting its characteristics to the surrounding environment. The idea is to combine the cognitive radio and the IR-UWB technologies in a way that the benefits of both are jointly explored. From this perspective, what is written in [9] can be interpreted not as a specific application, but as a starting discussion on the applicability, benefits and research challenges of the cognitive IR-UWB radio approach.

The authors in [10] explore the use of cognitive technology to enable the operation of UWB impulse radio devices in WiMax bands, under the strategy of detection and avoidance (DAA) of WiMax devices. The detection part is a typical spectrum sensing problem in cognitive radio (secondary) networks, and can be formulated as a binary hypothesis testing, where the aim is to distinguish between the presence and the absence of the primary transmitted signal in the sensed band. The avoidance part requires a UWB device to cease transmission and/or reduce transmit power in the bands where a WiMax link is detected.

In [11] it is also addressed the strong synergy between the aims of cognitive radio and features of UWB, especially of UWB impulse radio. Grounded on the well-accepted claim that UWB-based impulse radio CR is considered one of the best candidates for future short range wireless communication technology, the authors in [11] address how the CR features can be applied to the IR-UWB technology.

C. IR-UWB in Imaging Systems

The UWB impulse radio technology can be used in wall, through-wall and ground-penetrating radar (GPR) imaging, as well as in imaging systems for medical applications [3, p. 206][4]. Wall and GPR devices send IR-UWB signals into the wall or down into the ground, respectively, with the purpose of detecting or obtaining images of objects within the wall, or buried. GPR applications also include the determination of the physical properties within the ground. Those devices typically operate below 960 MHz, or in the frequency band of 3.1 to 10.6 GHz. Through-wall imaging devices typically operate below 960 MHz, or in the frequency band of 1.99 to 10.6 GHz, and can detect the location or movement of persons or objects on the other side of a wall. In medical imaging, IR-UWB pulses are sent through the bodies of persons or animals to produce images of their interior. In all of the above imaging applications the sensors are based on field disturbance.

D. IR-UWB in Measuring Systems

As opposed to narrowband signals, UWB impulse radio signals have the capability of accurate distance and positioning measurements. Besides communications and imaging, those measuring features sustain one of the most envisaged applications of IR-UWB [4].

E. IR-UWB in Vehicular Radar

IR-UWB has an available vehicular radar band for use in collision avoidance and parking aids devices. These devices are able to detect the location and movement of objects near a vehicle, also enabling features such as improved air bag activation and suspension systems [3, p. 193, 199][4].

VI. Concluding Remarks

In this paper we have addressed some introductory concepts about the IR-UWB technology, including transmit pulse construction, signaling formats, channel models, reception strategies and applications. Although the IR-UWB technology is not new, it was recently rediscovered and has proved to be adequate to a wide range of applications and as a strong candidate for current and future communication systems. It is really an idea whose time has come.

Throughout the presentation of the text, we have only mentioned two multiple-access techniques: time-hopping and direct-sequence. We have not mentioned any technique for medium access control (MAC). The interested reader can find additional information on MAC techniques applied to UWB systems in [12, pp. 123-125], [14], [15], [16, Chaps. 13, 14], [18, Chap. 7], [19, Sec. 9.3], [66], and in references therein.

Other critical aspects of IR-UWB communications not discussed in this paper are channel estimation and synchronization. These subjects can be found in [16, Chap. 2],

[18, pp. 75-85], [19, Chap. 4], [67] and [68].

For the reader interested in complementing the content presented here, we recommend the papers [1], [3], [14] [15] and [21], and the books [12], [16], [17], [18], [19] and [20]. Papers from the special issue of the IEEE Transactions on Vehicular Technology on UWB are also worth reading [22].

REFERENCES

[1] WIN, M. Z. and SCHOLTZ, R. A. Impulse radio: How it works, IEEE Communications Letters, vol. 2, pp. 36-38, February 1998.

[2] ALLEN, B. et al (Editors). Ultra-Wideband Antennas and Propagation for Communications, Radar and Imaging. Chichester, England: John Wiley & Sons, Ltd., 2007.

[3] SIWIAK, K. and HUCKABEE, L. L. Ultrawideband Radio. In: Wiley Encyclopedia of Telecommunications (J. G. Proakis, ed.), Hoboken, New Jersey, USA: John Wiley & Sons, Inc., Vol. 5, pp. 2754-2762. 2003.

[4] FCC-02-48 Report and Order: Revision of Part 15 of the Commission's Rules Regarding Ultra-Wideband Transmission Systems. April 2002.

[5] SCHMIDT, M. and JONDRAL, F. Ultra Wideband Transmission Based on MC-CDMA. Proc. IEEE GLOBECOM, 2003, pp. 749-753, December 2003.

[6] CHONG, C.-C., WATANABE, F. and INAMURA, H. Potential of UWB Technology for the Next Generation Wireless Communications. In: Proceedings of the ninth ISSSTA, 2006.

[7] IEEE Std. 802.15.4a. PART 15.4: Wireless Medium Access Control (MAC) and Physical Layer (PHY) Specifications for Low-Rate Wireless Personal Area Networks (WPANs): Amendment 1: Add Alternate PHYs. August 2007.

[8] ALBERTS, M., Analysis of the IEEE 802.15.4a ultra wideband physical layer through wireless sensor network simulations in OMNET++, MEng dissertation, University of Pretoria, Pretoria, Available: http://upetd.up.ac.za/thesis/available/etd-03102011-122128, 2011.

[9] GRANELLI, F., and H ZHANG. Cognitive Ultra Wide Band Radio: a Research Vision and its Open Challenges. Ultra Wide Band and Workshop on Ultra Wide Band. 2005. pp. 55- 59.

[10] MISHRA, S. M., ten BRINK, S., MAHADEVAPPA, R. and BRODERSEN, B. Cognitive Technology for Ultra-Wideband/WiMax Coexistence. IEEE DySpan Conference, April, 2007.

[11] AL-MAMUN, A. and ULLAH, M. R. Cognitive Radio for Short Range Systems based on Ultra-Wideband. M.Sc. Dissertation, Blekinge Institute of Technology, 2011.

[12] GHAVAMI, M., MICHAEL, L. B. and KOHNO, R. Ultra Wideband Signals and Systems in Communication Engineering. 2nd Ed. Chichester, England: John Wiley & Sons, Ltd., 2007.

[13] GUIMARÃES, D. A., Digital Transmission: A Simulation-Aided Introduction with VisSim/Comm. Berlin-Heidelberg, Germany: Springer-Verlag, Inc., 2009.

[14] SCHOLTZ, R. A. Multiple Access with Time-Hopping Impulse Modulation. In: Proc. IEEE Mil. Commun. Conf. (MILCOM), vol. 2, Maryland, USA, pp. 447-450, October 1993.

[15] WIN, M. Z. and SCHOLTZ, R. A. Ultra-Wide Bandwidth Time-Hopping Spread-Spectrum Impulse Radio for Wireless Multiple-Access Communications. IEEE Trans. Communications, vol. COM-48, pp. 679-691, April 2000.

[16] ARSLAN, H., CHEN, Z. N. and Di BENEDETTO, M.-G. Ultra Wideband Wireless Communication. New Jersey, USA: John Wiley & Sons, Inc., 2006.

[17] Di BENEDETTO, M.-G, KAISER, T., MOLISCH, A. F., OPPERMANN, I., POLITANO, C. and PORCINO, D. (Editors). UWB Communication Systems – A Comprehensive Overview. New York, USA: Hindawi Publishing Corp., 2006.

[18] OPPERMANN, I, HÄMÄLÄINEN, M. and IINATTI, J. UWB Theory and Applications. Chichester, England: John Wiley & Sons, Ltd., 2004.

[19] SHEN, X., GUIZANI, M., QIU, R. C., and Le-NGOC, T. Ultra-Wideband Wireless Communications and Networks. Chichester, England: John Wiley & Sons Ltd., 2006.

[20] SIWIAK, K. and McKEOWN, D. Ultra-Wideband Radio Technology. Chichester, England: John Wiley & Sons Ltd., 2004.

[21] YANG, L. and GIANNAKIS, G. B. Ultra-Wideband Communications – An Idea Whose Time has Come. IEEE Signal Processing Magazine, pp.26-54, November 2004.

[22] QIU, R. C., SCHOLTZ, R. and SHEN, X. Ultra-Wideband Wireless Communications – A New Horizon. Editorial of: IEEE Trans. Vehicular Technology, Vol. 54, no. 5. September 2005.

[23] DURISI, G. and BENEDETTO, S. Performance Evaluation and Comparison of Different Modulation Schemes for UWB Multiaccess Systems. Proc. IEEE ICC, 2003, pp. 2187-2191, May 2003.

[24] HU, B and BEAULIEU, N. C. Accurate Evaluation of Multiple-Access Performance in TH-PPM and TH-BPSK UWB Systems. IEEE Trans. Communications, vol. COM-52, pp. 1758-1766, October 2004.

[25] LIANG, B., GUNAWAN, E., LAW, C. L. and THE, K. C. Accurate Bit-Error Rate Evaluation for TH-PPM Systems in Nakagami Fading Channels Using Moment Generating Functions. IEICE Trans. on Communications, Vol. E91-B, No.3, pp. 922-926, March 2008.

[26] SAAD, P. BOTTERON, C., MERZ, R, and FARINE, P.-A. Performance Comparison of UWB Impulse-Based Multiple Access Schemes in Indoor Multipath Channels. In: proceedings of the 5th WPCN'08. Hannover, Germany, pp. 89-94, March 2008.

[27] SIMON, M. K. and ALOUINI, M.-S. Digital Communications over Fading Channels. 2nd Ed. New Jersey, USA: John Wiley & Sons, Inc., 2005.

[28] PROAKIS, J. G. and SALEHI, M. Fundamentals of Communication Systems. Upper Saddle River, New Jersey, USA: Prentice-Hall, Inc., 2005.

[29] CASSIOLI, D.,WIN, M. Z. and MOLISCH, A. F. The Ultra-Wide Bandwidth Indoor Channel: From Statistical Model to Simulations. IEEE Journal Selected Areas in Comm., vol. 20, pp. 1247-1257, August 2002.

[30] MOLISCH, A. F. et al. A Comprehensive Standardized Model for Ultrawideband Propagation Channels. IEEE Transactions on Antennas and Propagation. Vol. 54, No. 11, pp. 3151-3166, 2006.

[31] COST 231 – Final Report. Digital Mobile Radio Towards Future Generation Systems. Brussels, Belgium, 1997.

[32] HASHEMI, H. Impulse Response Modeling of Indoor Radio Propagation Channels. IEEE Journal Selected Areas in Comm., vol. 11, pp. 967-978, September 1993.

[33] MATIJN, E. (Ed.) State of the Art Channel Models. Report BTS01063 - Deliverable D2.1. Broadband Radio@Hand. TU Eindihoven. 2002.

[34] RUBIO, L. M. et al. Channel Modeling and Characterization at 17 GHz for Indoor Broadband WLAN. IEEE J. Select. Areas Commun, vol. 20, No. 3, pp. 593-601, April 2002.

[35] SALEH, A. A. M. and VALENZUELA, R. A Statistical Model for Indoor Multipath Propagation, IEEE J. Select. Areas Commun., Vol. SAC-5, No. 2, pp. 128-137, February 1987.

[36] HASHEMI, H. The Indoor Radio Propagation Channel. Proceedings of the IEEE, Vol. 81, No. 7, pp. 943-968, July 1993.

[37] LANDSTORFER, F., WOELFLE, G. and HOPPE, R. Propagation Models for Indoor Communications. In: Wiley Encyclopedia of Telecommunications (J. G. Proakis, ed.), vol. 4. Hoboken, New Jersey, USA: John Wiley & Sons, Inc., pp. 2012-2021, 2003.

[38] DURANTINI, A., CICCOGNANI, W. and CASSIOLI, D. UWB Propagation Measurements by PN-Sequence Channel Sounding. Proc. IEEE ICC, 2004, pp. 3414-3418, June 2004.

[39] FOERSTER, J. R. and LI, Q. UWB Channel Modeling Contribution from Intel. IEEE P802.15 Working Group for WPANs. August 2008.

[40] GHASSEMZADEH, S. S., JANA, R., RICE, C. W., TURIN, W. and TAROKH, V. Measurement and Modeling of an Ultra-Wide Bandwidth Indoor Channel. IEEE Trans. Communications, vol. COM-52, pp. 1786-1796, October 2004.

[41] MOLISCH, A. F. Ultrawideband Propagation Channels – Theory, Measurement, and Modeling. IEEE Transactions on Vehicular Technology. Vol. 54, Issue 5, pp. 1528-1545, September 2005.

[42] MUQAIBEL, A. H. Characterization of Ultra Wideband Communication Channels. Ph.D. Thesis, Virginia Polytechnic Institute and State University, 2003.

[43] RAPPAPORT, T. S. Wireless Communications, 2nd Ed. Upper Saddle River, New Jersey, USA: Prentice-Hall, Inc., 2002.
[44] ROSSI, J. P. and Y. GABILLET, Y. A Mixed Ray Launching/Tracing Method for Full 3-D UHF Propagation Modeling and Comparison with Wide-Band Measurements. IEEE Trans. on Ants. and Prop., Vol. 50, No. 4, pp. 517-523, April 2002.
[45] WHITTEKER, J. H. Physical Optics and Field-Strength Predictions for Wireless Systems. IEEE J. Select. Areas Commun. Vol. 20, No. 3, pp. 515-522, April 2002.
[46] ANDERSEN, J. B., RAPPAPORT, T. S. and YOSHIDA, S. Propagation Measurements and Models for Wireless Communications Channels, IEEE Communications Magazine. Vol. 33, pp. 42-49, January 1995.
[47] ISKANDER, M. F. and YUN, Z. Propagation Prediction Models for Wireless Communication Systems. IEEE Trans. Microwave Theory and Techniques. Vol. 50, No. 3, pp. 662-673, March 2002.
[48] NESKOVIC, A., NESKOVIC, N. and PAUNOVIC, G. Modern Approaches in Modeling of Mobile Radio Systems Propagation Environment. IEEE Commun. Surveys, Vol. 3, pp. 2-12, 2000.
[49] SARKAR, T. K. et al., A Survey of Various Propagation Models for Mobile Communication, IEEE Antennas and Propagation Magazine, Volume 45, Issue 3, pp. 51-82, June 2003.
[50] IEEE VT-S Propagation Committee. Wireless Planning Tools for Mobility and Indoor Systems. Available in: http://members.shaw.ca/propagation/ (last access on May 2009).
[51] CORREIA, L. M. (Ed.). Wireless Flexible Personalised Communications COST 259. European Co-operation in Mobile Radio Research. New York, USA: John Wiley and Sons, Inc., 2001.
[52] ITU-R Rec. P. 1411-3. Propagation Data and Prediction Methods for the Planning of Short-range Out-door Radiocommunication Systems and Radio Local Area Networks in the Frequency Range 300MHz to 100 GHz. ITU Radiocommunication Assembly: Geneva, 2005.
[53] KITAO, K. and ICHITSUBO, S. Path Loss Prediction Formula in Urban Area for the Fourth-Generation Mobile Communication Systems. IEICE Trans. Commun., Vol. E91–B, No. 6, pp. 1999-2009, June 2008.
[54] SIWIAK, K. Radiowave Propagation and Antennas for Personal Communications. Norwood, MA, USA: Artech House, Inc. 1995.
[55] GOLDSMITH, A. Wireless Communications. New York, USA: Cambridge University Press, 2005.
[56] JAKES, W. C. (Ed.) Microwave Mobile Communications. New York, USA: IEEE Press, 1994.
[57] VALENZUELA, R. Ray Tracing Prediction of Indoor Radio Propagation. In: Proceedings of PIMRC '94, pp. 140-143, The Hague, The Netherlands, 1994.
[58] JANSSEN, G. J. M., STIGTER, P. A. and PRASAD, R. Wideband Indoor Channel Measurements and BER Analysis of Frequency Selective Multipath Channels at 2.4, 4.75, and 11.5 GHz. IEEE Trans. Communications, vol. COM-44, pp. 1272-1288, October 1996.
[59] PROAKIS, J. G. Digital Communications. 3rd Ed. USA: McGraw Hill, Inc., 1995.
[60] CHAO, Y.-L. and SCHOLTZ, R. A. Ultra-Wideband Transmitted Reference Systems. IEEE Trans. on Vehicular Technology. Vol. 54, Issue 5, pp. 1556-1569. September 2005.
[61] GUO, N., SADLER, B. M. and QIU, R. C. Reduced-Complexity UWB Time-Reversal Techniques and Experimental Results. IEEE Transactions on Wireless Communications, Vol. 6, No. 12, pp. 4221-4226, December 2007.
[62] NGUYEN, H. T., ANDERSEN, J. B., PEDERSEN, G. F., KYRITSI, P. and EGGERS, P. C. F. Time Reversal in Wireless Communications: A Measurement-Based Investigation. IEEE Transactions on Wireless Communications, Vol. 5, No. 8, pp: 2242-2252, August 2006.
[63] NGUYEN, H. T., KOVACS, I. Z. and EGGERS, P. C. F. A Time Reversal Transmission Approach for Multiuser UWB Communications. IEEE Transactions on Antennas and Propagation. Vol. 54, No. 11, Part 1, pp. 3216-3224. November 2006.
[64] STROHMER, T., EMAMI, M., HANSEN, J., PANANICOLAOU, G. and PAULRAJ, A. J. Application of Time-Reversal with MMSE Equalizer to UWB Complications. Proc. IEEE Globecom'04, Dallas, TX, December 2004.
[65] ROUSEFF D. et al. Underwater Acoustic Communication by Passive-Phase Conjugation: Theory and Experimental Results. IEEE Journal of Oceanic Engineering. Vol. 26, No. 4, pp. 821-831. 2001.
[66] SHEN, X., ZHUANG, W., JIANG, H. and CAI, J. Medium Access Control in Ultra-Wideband Wireless Networks. IEEE Trans. on Vehicular Technology. Vol. 54, Issue 5, pp. 1663-1677. September 2005.
[67] AEDUDODLA, S. R., VIJAYAKUMARAN, S. and WONG, T. F. Timing Acquisition in Ultra-Wideband Communication Systems. IEEE Trans. on Vehicular Technology. Vol. 54, Issue 5, pp. 1570-1583, September 2005.
[68] CARBONELLI, C, MENGALI, U. and MITRA, U. Synchronization and Channel Estimation for UWB Signals. Proc. IEEE GLOBECOM, 2003, pp. 764-768, December 2003.

Dayan Adionel Guimarães was Born in Carrancas, MG, Brazil, on March 01, 1969. He holds the titles: Electronics Technician (ETE FMC, 1987), Electrical Engineer (Inatel, 1994), Specialist in Data Communication Engineering (Inatel, 2003), Specialist in Human Resources Management (FAI, 1996), Master in Electrical Engineering (Unicamp, 1998) and Doctor in Electrical Engineering (Unicamp, 2003). In 2010 he attended a Pos-Doctoral internship at Federal University of Santa Catarina (UFSC), studying Spectrum Sensing for Cognitive Radio applications and Convex Optimization.

From 1988 to 1993 he developed equipment for Industrial Instrumentation and Control, and also occupied the positions of Manufacturing and Product Engineering Supervisor at *SENSE Sensores e Instrumentos*. Since January 1995 he is Professor at Inatel where, for eight years, he was responsible for the structure that supports practical teaching activities for the Electrical Engineering undergraduate course. His research includes the general aspects of Digital Transmission and Mobile Communications. He is currently working on Eigenvalue-Based Spectrum Sensing for Cognitive Radio.

Dr. Dayan is member of the *Telecomunicações* magazine's Editorial Board, member of the Inatel's Master Degree Counseling Board and of the IEICE *(Institute of Electronics, Information and Communication Engineers*), Japan.

Geraldo Gil Ramundo Gomes graduated in Telecommunications Operation Engineering (1979) and in Electrical Engineering, Option Electronics (1981) at National Institute of Telecommunications, Inatel, Brazil. He obtained his Master degree in Electrical Engineering, Electronics and Communications areas (1997) and their Doctorate in Electrical Engineering, Telecommunications and Telematics areas (2002) in the Faculty of Electrical and Computer Engineering, State University of Campinas - UNICAMP. In 2010 he attended a Pos-Doctoral internship at Federal University of Santa Catarina (UFSC), studying Cooperative Coding for Cognitive Radio applications. He is currently a professor of the National Institute of Telecommunications and holds a Category 2 Product Certification by NCC Brazil, for ANATEL. He also occupied the positions of P&D Engineer and P&D Engineering Manager at Linear Equipamentos Eletrônicos S.A. (1985-1991). His areas of interest include: Digital Communication Systems, Terrestrial and Satellite Radio Link Systems, and Digital TV Systems. Dr. Geraldo Gil is an IEEE CommSoc Member.